Refining of Si-Ca-Al alloys using slag treatments.

E. Emil-Kaya[1], F. Sørli[2], M. Wallin[3] and G. Tranell[4]

1.Postdoctoral Researcher, Norwegian University of Science and Technology, Trondheim, Norway 7034. Email: elif.e.kaya@ntnu.no
2. Former MSc student, Norwegian University of Science and Technology, Trondheim, Norway 7034. Email: Fredrik.sorli@ntnu.no
3. Researcher, Norwegian University of Science and Technology, Trondheim, Norway 7034. Email: maria.wallin@ntnu.no
4. Professor, Norwegian University of Science and Technology, Trondheim, Norway 7034. Email: gabriella.tranell@ntnu.no

Keywords: aluminothermic reduction, silicon refining

ABSTRACT

Silicon has been classified as a critical raw material (CRM) by the European Union since 2014, owing to its high supply risk and significant economic importance. Silicon (Si) is a pivotal element in products that surround us every day, such as electronics, solar panels, and various chemical applications. The demand for a sustainable and circular silicon value chain is becoming increasingly urgent. State-of-the-art metallurgical grade silicon (MG-Si) production is achieved through carbothermic reduction of quartz, typically emitting >4.8 tonnes of CO_2/tonne Si. An alternative method for Si production is aluminothermic reduction of SiO_2 in a SiO_2-CaO slag, employing aluminium by-products such as aluminium Al-dross and Al-scrap as reductants, offering a process without direct carbon emissions. The process produces a Si-Ca-Al alloy and a $CaO\text{-}Al_2O_3$ slag with small amounts of residual SiO_2.

The present study investigates the refining of a $Si_{75}\text{-}Ca_{15}\text{-}Al_{10}$ alloy obtained from aluminothermic reduction, using different slags in scales from gram to hundred kilo scales. Different slag compositions and materials such as slag sculls, anorthosite and pre-fused $CaO\text{-}SiO_2$ slags were used. The experimental studies were supplemented by thermodynamic modelling using FactSage 8.2.

The results show that slag refining can be a fast and effective way of transferring Ca and Al to a slag phase, resulting in a >98% pure Si with high Si yield. Elemental mass balances and metal/slag analyses largely agree with thermodynamic modelling results.

INTRODUCTION

Silicon (Si) plays a crucial role in various sectors such as aluminium alloy industry (Dong and Lv, 2021), semiconductor industry (Taeko and Fu, 2019), organic silicon industry (Bok and Jung, 2004) and photovoltaic industry (Hsu, Wu, and Lu, 2014). It is foreseen that the solar photovoltaic (PV) sector will undergo significant growth, expecting an average annual installation increase of 25% between 2022 and 2030. To achieve net-zero emissions by 2050, a substantial increase, amounting to twelve times the current capacity, in polysilicon production capacity is considered essential (Solar PV, IEA, Paris, PV magazine, 2022). The commercial production of metallurgical grade Si (MG-Si) is performed through carbothermic reduction of quartz in a submerged arc furnace, and this process generates high amount of greenhouse gas. The considerable energy demand associated with this method can lead to substantial emissions, particularly when utilizing fossil-based energy sources (Sævarsdottir, Kvande, and Magnusson, 2021). Currently, metallurgical methods for purifying Si to 99% purity and beyond include oxidative (gas) refining (Bjørnstad and Tranell, 2021; Kero et. al, 2015), directional solidification (Martorano et al. 2011), slag refining (Wei et al. 2023, Zhou et al. 2019, Hosseinpour and Tafaghodi Khajavi, 2018), vacuum refining (Zheng et al., 2011, Ren, Wand and Morita, 2018, Hoiseinpur and Safarian, 2021), electron beam processes (Tan et al., 2013), leaching (Zhang et al., 2013 Zhu et al., 2021, Fan et al., 2014) and others. MG-Si typically exhibits a purity level exceeding 99%, with primary impurities being Al, Fe, and Ca. From a thermodynamic perspective, Al, Mg, Ba, and Ca exhibit a higher affinity towards oxygen when compared to Si. Consequently, these elements are prone to oxidize and are separated from Si during slag formation and treatment.

The Oxidative Ladle Refining (OLR) method is extensively employed in the industrial production of MG-Si. This process involves purging the liquid alloy with oxygen-enhanced air at temperatures ranging from 1823 K to 1873 K. This initiates reactions with Si and the primary impurities forming a SiO_2 -$CaO\text{-}Al_2O_3$ slag. Bjørnstad and Tranell, 2021 developed a thorough theoretical explanation of slag nucleation and formation on the nano/microscale by employing classical macroscale thermodynamics. They highlighted the surface-active properties of silica within the SiO_2 -$CaO\text{-}Al_2O_3$ system. Additionally, it demonstrated that elevating the calcia concentration in the slag has a more pronounced impact on the interfacial tension between the molten slag and liquid alloy compared to alumina. This finding validates industrial observations regarding the correlation between refining rates and the relative composition of alloy/slag. Bjørnstad et al., 2022 replicate the industrial process,

using five different alloy compositions, each with varying initial concentrations of Ca and Al. Samples were collected at 0, 5, 7, 10, and 15 minutes at a temperature of 1873 K. A model based on FactSage was employed to analyse the underlying thermodynamic system behaviour. The findings suggest that OLR of MG-Si follows three main steps: initially, the formation of slag through surface oxidation and purge gas, followed by the depletion of dissolved Ca in the melt, and subsequently, the formation of a silica-rich slag. Johnston and Barati (2010) examined the extraction of Fe, K, Ca, Mg from Si via slag treatment. They explored the impact of slag basicity on the partition ratio of these impurities at a temperature of 1773 K, employing different combinations of 20% Al_2O_3–BaO–SiO_2 mixtures. In the last couple of decades, many studies have focused on slag refining as a means of reducing the boron content in silicon for PV applications. Jakobsson and Tangstad (2014) conducted a study on the elimination of B from Si using ternary slags composed of CaO–MgO–SiO_2 and CaO–Al_2O_3–SiO_2. Their findings revealed that altering the quantity of CaO or MgO in the CaO–MgO–SiO_2 ternary had minimal impact on the partition ratio of B. Teixeira and Morita (2009) employed CaO–SiO_2–CaF_2 and CaO–SiO_2–Na_2O ternary slags to expand the basicity range at a temperature of 1823 K. They investigated the impact of basicity on Si refining by introducing 25 and 40 wt% CaF_2 to the CaO–SiO_2 binary system. The research indicated that increasing the basicity through the addition of CaF_2 did not exhibit a significant impact on B removal when compared to the CaO–SiO_2 binary system. Conventional slag compositions have consistently been favoured and commonly utilized in the Si refining process.

In this study, Si alloy produced through aluminothermic reduction, as an alternative to the carbothermic reduction of quartz, was refined by slag treatment. Various materials and by-products from the Si industry have been assessed for their suitability as slag alternatives. First, in laboratory scale, the refining efficiency of natural anorthosite ($CaAl_2Si_2O_8$) and magnetically refined (removal of iron-based impurities) anorthosite was examined at different holding times. Subsequently, the study explored the potential use of Si sculls, a byproduct from the MG-Si industry, as the main refining slag. Furthermore, large-scale slag refining was implemented to evaluate the feasibility of employing the refining using slag sculls in an industrial setting.

MATERIALS AND METHOD

Materials

In the slag refining process, various slag compositions were used. Figure 1 illustrates the materials utilized in the slag refining processes and their compositions. The Si alloy employed in the experiments was produced through the SisAl process (www.sisal-pilot.eu) and is henceforth referred to as SisAl metal. The aluminium used in the procedure comes from aluminium scrap. The Si sculls employed in this study are by-products obtained from the Si industry. Anorthosite is not typically used in the traditional silicon refining process. In this study, the feasibility of employing anorthosite and sculls as a slag in Si refining has been demonstrated.

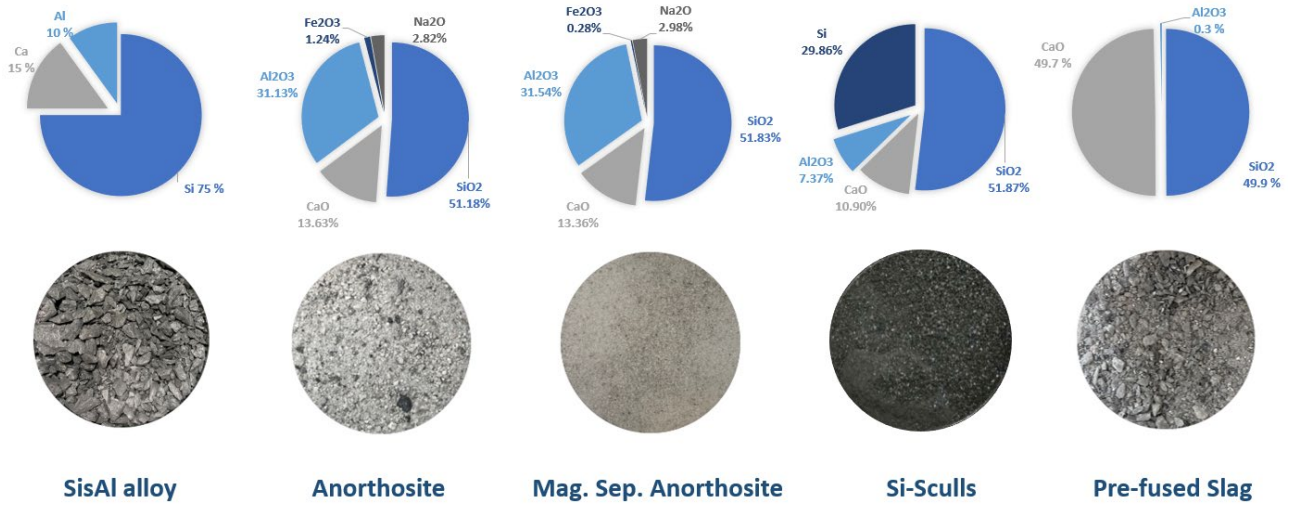

FIG 1 – Composition and image of the materials employed in the slag refining.

Experimental Procedures

Small-Scale Experiments

The specified quantities of slag and SisAl metal, as given in Table 1, were loaded into a small graphite crucible (H: 5.5cm, D_{inner}= 3.0 cm, D_{outer} 4.0). This charged crucible was then placed inside a larger graphite crucible susceptor (H: 15cm, D_{inner}= 6.9 cm, D_{outer} 8.5). To ensure efficient insulation within the furnace, layers of mica foil and graphite wool were inserted on the inner side of the coil. The thermocouple was shielded by an alumina tube and positioned adjacent to the small crucible within the large crucible. The assembly, including the small and large crucibles, was then introduced into the insulated coil of a vacuum induction furnace. The furnace was sealed and subjected to vacuum conditions, followed by purging with argon gas to establish an inert atmosphere during the experiment. The atmospheric pressure within the furnace was maintained in a stable range of 1040-1060 mbar. Following the preparation of the setup, the furnace was gradually heated up to 1600°C. After the specified holding time, the furnace was powered off and allowed to cool down for several hours. To ensure the integrity of the sample and prevent contamination, the furnace underwent vacuum conditions once again. Subsequently, air was reintroduced into the furnace to open it for the handling of the sample.

Table 1: Experimental parameters for small- and large-scale refining experiments.

Small-scale slag refining			
Codes	**Slag**	**Slag Basicity**	**Holding Time (min)**
Slag1	Anorthosite	0.25	10, 20, 30, 40, 50, 60
Slag2	Mag. Separated Anorthosite	0.25	10, 20, 30, 40, 50, 60
Slag3	Sculls w. Silicon	0.18	10, 20, 30, 40, 50, 60
S1	30-gram Sculls without Silicon	0.18	60
S2	30g Sculls without Silicon + 2g CaO	0.29	60
S3	20g Sculls without Silicon + 2g CaO	0.35	60
S4	20g Sculls without Silicon + 4g CaO	0.52	60
S5	20g Sculls without Silicon + 4g pre-fused slag	0.30	60

S6	20g Sculls without Silicon + 2g CaO + 4g pre-fused slag	0.44	60
S7	20g Sculls without Silicon + 2gr CaO + 2gr Al_2O_3	0.30	60
Large-scale slag refining			
Codes	**Sculls: Metal: $CaCO_3$**	**Slag Basicity**	**Holding Time (min)**
Lscull1	2:1:0.1	0.23	60
Lscull2	2:1:0.1	0.23	60
Lscull3	2:1:0.2	0.28	60
Lscull4	2:1:0.2	0.28	60

Large-Scale Trials

Large-scale trials were carried out using a 600-kW induction furnace equipped with a water-cooling system. Within the furnace, a graphite crucible with a volumetric capacity of 234 litres was accommodated. The material was weighed in buckets of 10-15 kg, where charging was done by half or full buckets on the furnace top through an opening in the lid. The furnace was charged with sculls initially. This was melted over a period of 7 hours. Afterwards, SisAl metal and pre-fused slag was charged every other time over a period of 2 hours. The furnace included a removable lid with a small hatch for manual charging, which was manipulated by a custom-built robot to ensure precision and safety before the tapping process. The tapping process was facilitated through a hydraulic furnace tilting system. The operational power was adjusted between 100 and 160 kW to maintain the melt temperature within the range of 1560-1590 °C. Table 1 provides an overview of the operational details for the large-scale slag refining. Temperature measurements were conducted by a Type-C thermocouple positioned near the centre of the slag melt. The melt was primarily agitated by purging nitrogen gas through a top lance, complemented by the induction-induced movement of the melt. Casting of metal and slag was done after a holding time of 60 minutes.

Liquid samples, weighing approximately 150 g each round, were taken during the large-scale trials. These collected liquid samples were fragmented and milled to obtain a particle size suitable for X-ray Fluorescence (XRF) analysis. The analysis employed the Wavelength Dispersive XRF (WD-XRF) technique on glass-fused beads, utilizing $LiBO_2$ and oxidizers through the FESIFLUX method. Additionally, solid samples were obtained from both the metal and slag. To maintain consistency, samples near the cast's edge were chosen, each weighing approximately 250 g. These solid samples were subsequently milled in preparation for XRF analysis.

RESULTS AND DISCUSSION

Small Scale Refining

In the refining process, all reactants initially move to and diffuse through the Si boundary layer, as indicated in Figure 2. Subsequently, the chemical reaction takes place at the interface, followed by the diffusion of products through the boundary layer into the corresponding bulk phase. Given the generally rapid rates of metallurgical chemical reactions at high temperatures, the process is often considered a rapid equilibrium phenomenon provided a high interfacial area for the reaction, facilitated by e.g gas or rotor stirring. The oxidization reaction's efficiency can be manipulated by various conditions, including slag composition and refining temperature (Zhang et al. 2013).

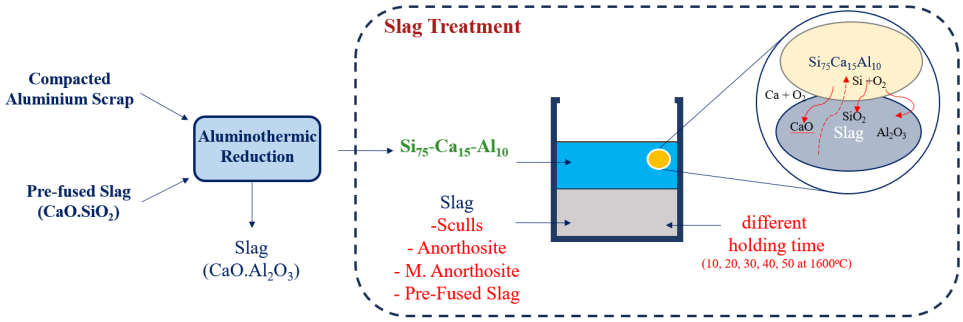

FIG 2 – Schematic representation of slag refining of SisAl metal produced through aluminothermic reduction.

Effect of different slag composition

The chemical composition of the produced alloys and slags after reaction with anorthosite, magnetically separated anorthosite, and sculls were examined through XRF analysis. Figure 3 illustrates the composition of Si metal refined with anorthosite, magnetically separated anorthosite, and sculls at different holding times (values are given in weight percent (wt.%). In the refining plots, the x-axis represents the holding times while the y-axis indicates the corresponding Si/impurity fraction. The composition analysis revealed that Si exhibited the highest variability in its composition, ranging from a minimum of 72 wt.% to a maximum of 98.97 wt.%, when utilizing sculls, anorthosite, and magnetically separated anorthosite at different holding times. Firstly, the refining of SisAl metal with anorthosite was examined, resulting in silicon with a content ranging from 72 wt.% to 98.2 wt.%, with a small amount of Fe. The introduction of Fe into the structure was attributed to the presence of Fe in composition of anorthosite. Additionally, the fractions of both Ca and Al remain consistently below 0.6 wt.% in all refining experiments. Magnetically separated anorthosite was investigated for the refining of SisAl metal, resulting in Si with a purity exceeding 98.7 wt.%. The refined alloy with magnetically separated anorthosite has, as expected, a lower Fe content compared to the one refined with anorthosite which can be attributed to the magnetic separation process. The high SiO_2 content in anorthosite and magnetically separated anorthosite ensure that there is no shortage of SiO_2 in the slag system, allowing a high Si concentration in the alloy (Engh T A, Sigworth G K, Kvithyld A, 2021). A smaller SiO_2 fraction in the slag system would alter the metal-slag equilibrium towards higher Ca and Al concentrations, sacrificing the Si purity. A significant CaO content (basicity) in the slag reduces the viscosity of the system which is favourable in terms of slag/metal surface tension and facilitates rapid mass transport. The initial CaO content in the two anorthosite refining slags was 13 wt.%, which is relatively low. However, the separation of the metal and slag phases in the crucible after the experiment was acceptable, indicating the CaO content at 13 wt.% was adequate.

This study also investigated the utilization of Si sculls, a by-product from the refining of tapped alloy in the carbon-based Si industry, as the primary refining slag. These sculls consist of a slag phase and a metallic Si phase, and their composition can vary from batch to batch. XRF analysis of the sculls used in the experiments indicated a metallic Si content of 30.4 wt.%, along with 52.8 wt.% SiO_2, 11.1 wt.% CaO, and 7.5 wt.% Al_2O_3, as shown in Figure 1. The refining of SisAl metal with sculls resulted in Si with a content ranging from 72 wt.% to 94.95 wt.%. This can be attributed to the higher relative quantities of CaO and Al_2O_3 in sculls compared to anorthosite and magnetically separated anorthosite. This significantly influences slag formation, leading to reduced metal purity.

To investigate the effect of slag basicity on the performance of the refining process, anorthosite, magnetically separated anorthosite, and sculls were compared. Anorthosite and magnetically separated anorthosite were classified with a relatively higher basicity of 0.25 compared to the basicity of sculls, which was 0.18. Notably, a lower basicity resulted in a lower content of Si metal.

Effect of holding time

To assess the refining rate, the SisAl alloy was refined using anorthosite, magnetically separated anorthosite, and sculls for 10, 20, 30, 40, and 60 minutes respectively. After a holding period of 10 minutes, the SisAl alloy was refined with anorthosite, achieving a purity of 97.5 wt%. These findings are consistent with the theoretical studies, implying the majority of the refinement takes place before the 10-minute threshold (Safarian and Tangstad, 2013). A 60-minute holding time resulted in the highest purity at 98.2 wt%. Nevertheless, the connection between holding time and purity is indiscernible from this plot, as metal sampling without slag inclusions is challenging, making exact compositional analysis prone to some error.

Al and Ca contents show a declining trend from 1.3-1.7 wt.% at a 10-minute holding time to below 0.5 wt.% with a 60-minute holding time, revealing the effect of holding time on impurity removal. The Fe content observed in the five individual experiments remained at high levels, as would be expected. The analysis reveals that Fe constitutes the majority of impurities, varying between 0.98 wt.% and 1.84 wt.%. The difference between the results of natural anorthosite and magnetically separated experiments is substantial.

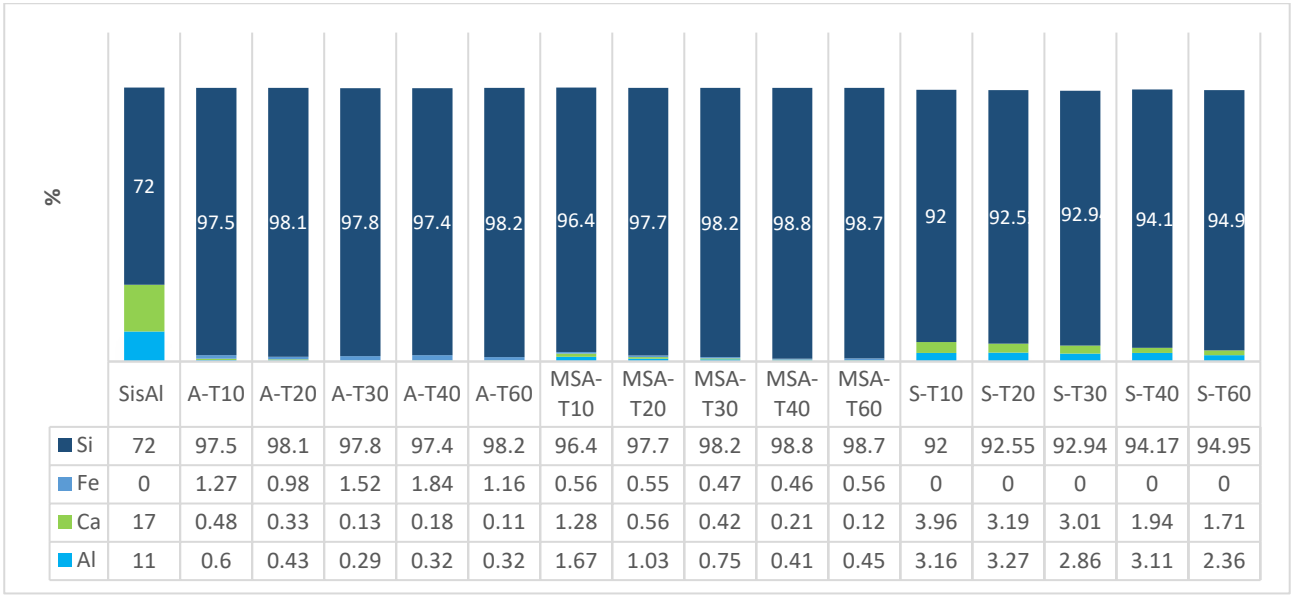

	SisAl	A-T10	A-T20	A-T30	A-T40	A-T60	MSA-T10	MSA-T20	MSA-T30	MSA-T40	MSA-T60	S-T10	S-T20	S-T30	S-T40	S-T60
Si	72	97.5	98.1	97.8	97.4	98.2	96.4	97.7	98.2	98.8	98.7	92	92.55	92.94	94.17	94.95
Fe	0	1.27	0.98	1.52	1.84	1.16	0.56	0.55	0.47	0.46	0.56	0	0	0	0	0
Ca	17	0.48	0.33	0.13	0.18	0.11	1.28	0.56	0.42	0.21	0.12	3.96	3.19	3.01	1.94	1.71
Al	11	0.6	0.43	0.29	0.32	0.32	1.67	1.03	0.75	0.41	0.45	3.16	3.27	2.86	3.11	2.36

(a)

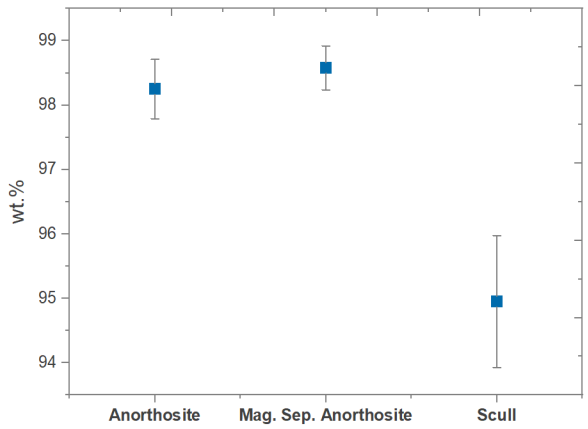

(b)

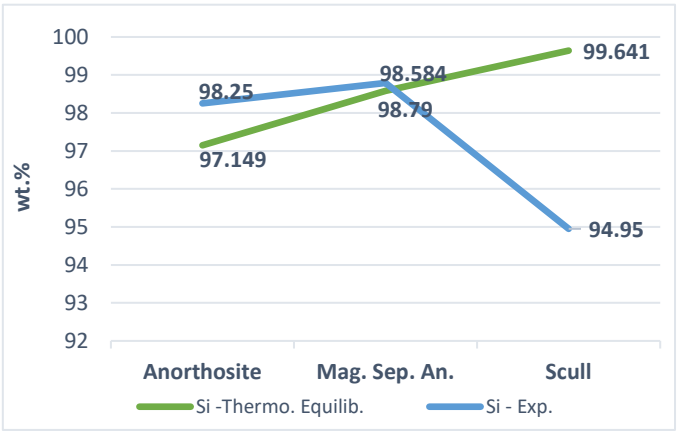

(c)

FIG 3 – (a) Composition of the refined SisAl alloys refined with anorthosite (A-T10 – A-T60), magnetically separated anorthosite (MSA-T10 – MSA-T60), and Sculls (S-T10 – S-T60) at different

holding times, (b) Si purity with error bars, (c) comparison of the experimental and predicted values.

The chemical composition analysis was conducted through multiple repetitions to ensure accuracy, and the obtained data were used to calculate error bars. In Figure 3 (c), the Si content is given alongside these error bars. The refining process with anorthosite and magnetically separated anorthosite shows considerable potential for Si refining.

The assessment of whether the experiments reached chemical equilibria is pivotal for evaluating the efficiency of the refining process. Equilibrium calculations were hence conducted through FactSage 8.2, utilizing the FTLite, FToxid, and FactPS databases for equilibrium calculations. Figure 3 (b) presents the comparison of the experimental results and the predicted values via FactSage 8.2. The composition of refined alloy with anorthosite and magnetically separated anorthosite align well with the predicted values. The observed deviation of the refined alloy with scull from the calculated values can be attributed to high Si content of sculls. Thermodynamic calculations indicated the formation of SiC, leading to comparatively less Si.

After the refining experiments, macro-microscopic investigations of the refined Si metal with anorthosite and mag. separated anorthosite was discovered. Figure 4 illustrates the cross section of samples refined with (a) anorthosite and (b) magnetically separated anorthosite at different holding times. Upon examining the cross-sections, a distinct boundary is observed between the slag and the alloy, with the slag positioned at the top of the crucible due to its lighter density. This is indicative of the successful slag and metal separation.

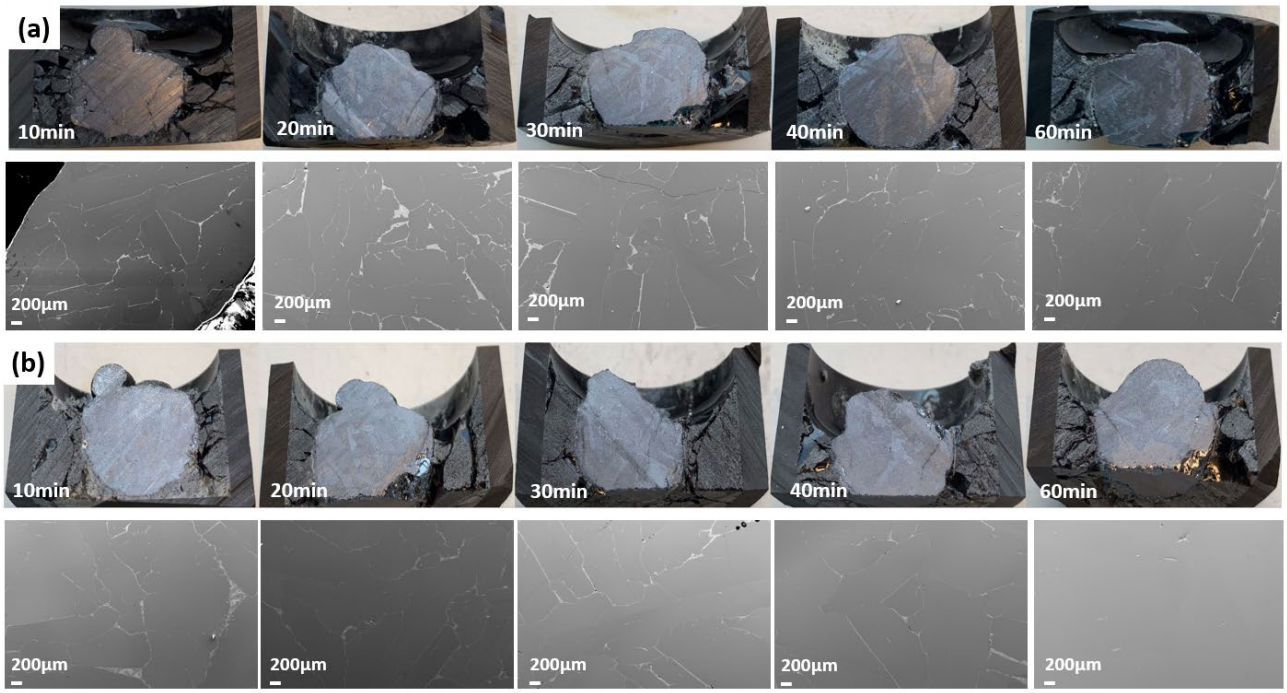

FIG 4 – Cross-section of the refined samples and microstructure in the alloys refined with (a) anorthosite and (b) mag. separated anorthosite at different holding times.

Metallic impurities in Si tend to segregate to the grain boundaries during the solidification process. This segregation is followed by the co-precipitation of these impurities as various intermetallic phases. The small segregation coefficients ($\ll 1$), as indicated in the literature (Zhu et al., 2022), contribute to this phenomenon. Figure 5 (a) illustrates distinct impurity regions present in the SisAl metal and, (b) and (d) microstructure and phases of the refined Si metal and (c) chemical composition of the selected points.

Notably, an examination of the impurity region on the right reveals the presence of three distinguishable phases: one primary Si phase and two intermetallic phases, one primarily Ca-Al-Si and one high Ca-Fe-Si phase. Detailed analysis of the phase compositions was conducted using energy-dispersive spectroscopy (EDS) point analysis, and the results are summarized in Figure 5 (c). This information sheds light on the chemical composition of these distinct phases within the impurity regions.

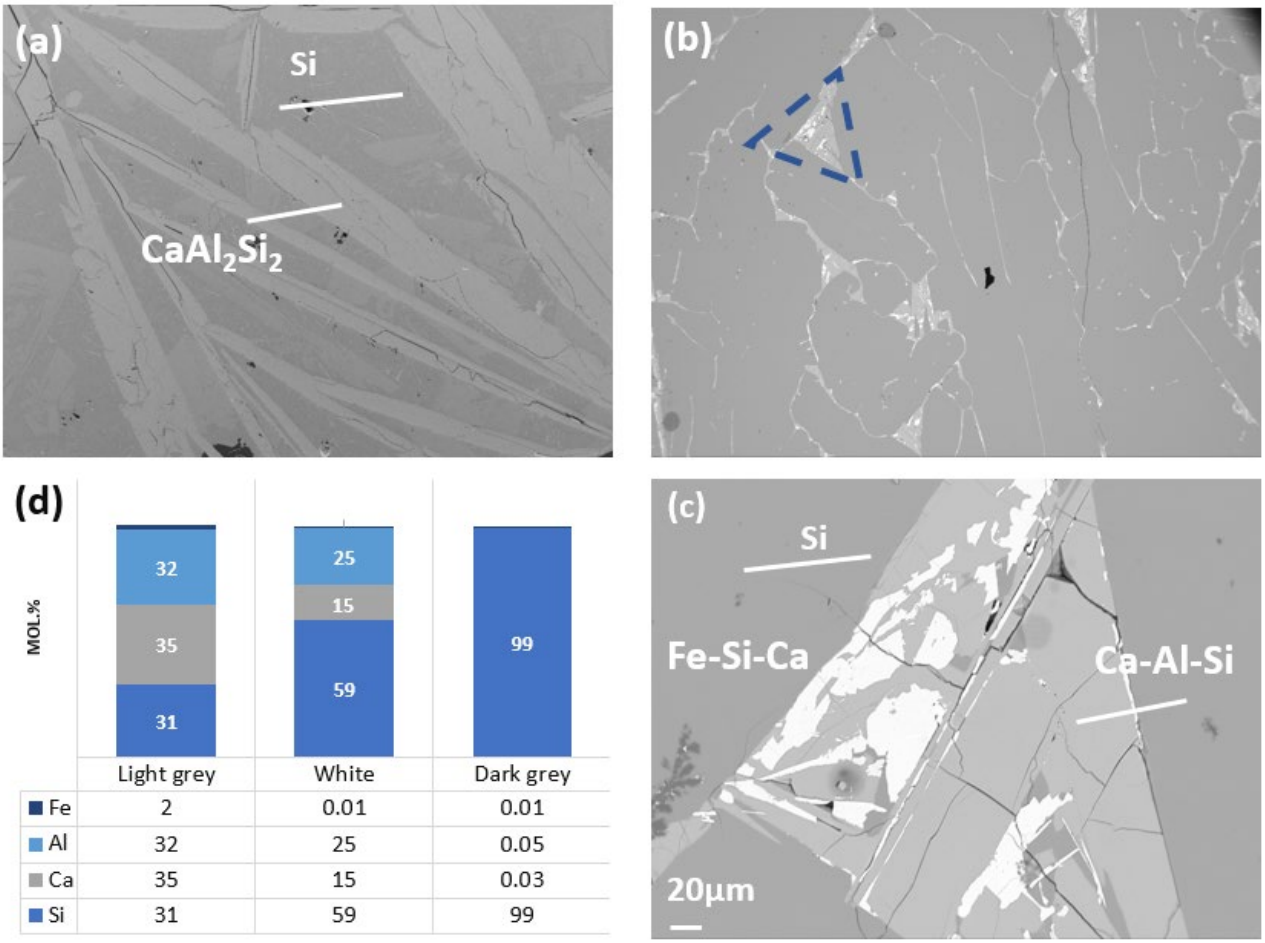

FIG 5 – Microstructure in (a) the SisAl metal and (b) and (c) the refined Si metal and (d) chemical composition of the selected points.

Effect of addition of CaO, Al_2O_3 and pre-fused slag

For further refining process optimization, sculls were melted, and Si removed. The melted slag-part of the sculls were then used in the subsequent refining process. The use of melted skulls led to an enhanced purity of the refined Si metal, ranging from 94.95 wt.% to 98.75 wt.%. The subsequent experiments investigated the influence of adding CaO, pre-fused slag, and/or Al_2O_3 on the purity of Si metal, and the results are depicted in Figure 6. While the addition of CaO resulted in Si with a purity of approximately 98 wt.%, the addition of pre-fused slag and Al_2O_3 resulted in Si with a purity of 97 wt.%. The addition of 4 grams of CaO and 4 grams of pre-fused slag resulted in the production of Si with a purity of about 95 wt.% and 98 wt.%, respectively. The addition of CaO in the slag lead to somewhat lower purity of Si metal; however, it facilitated slag-metal separation during casting.

To investigate the effect of slag basicity on the performance of the refining process with sculls, values of relatively lower and higher slag basicity were compared. The refining process with both high and low slag basicity showed lower refining performance in terms of Si metal purity and castability. Consequently, optimal refining results were achieved with slag basicity values between 0.25 and 0.35.

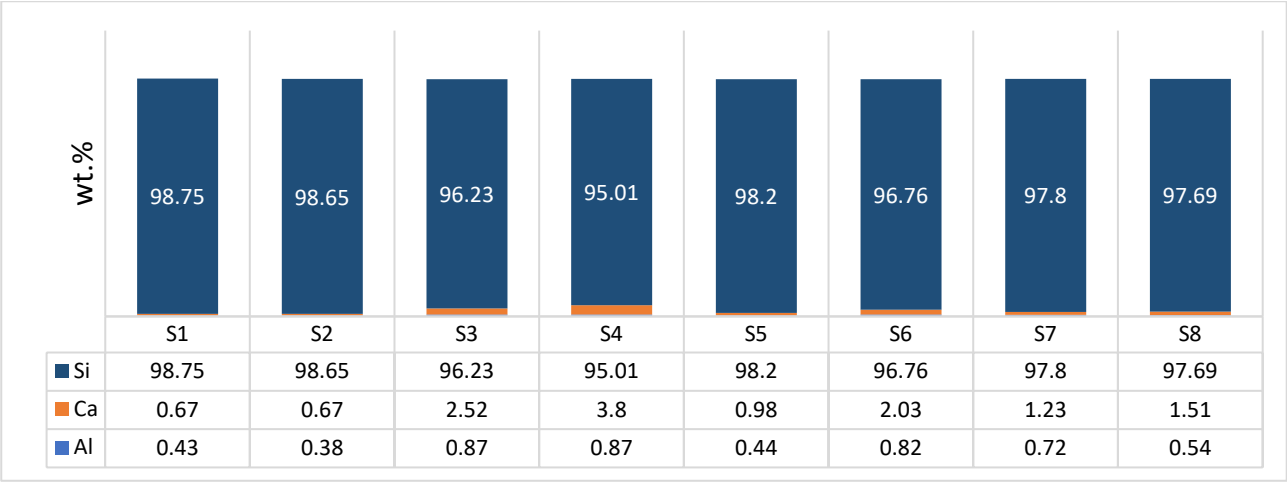

	S1	S2	S3	S4	S5	S6	S7	S8
Si	98.75	98.65	96.23	95.01	98.2	96.76	97.8	97.69
Ca	0.67	0.67	2.52	3.8	0.98	2.03	1.23	1.51
Al	0.43	0.38	0.87	0.87	0.44	0.82	0.72	0.54

(a)

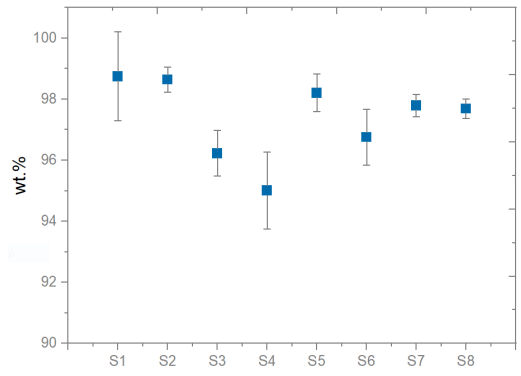

(b)

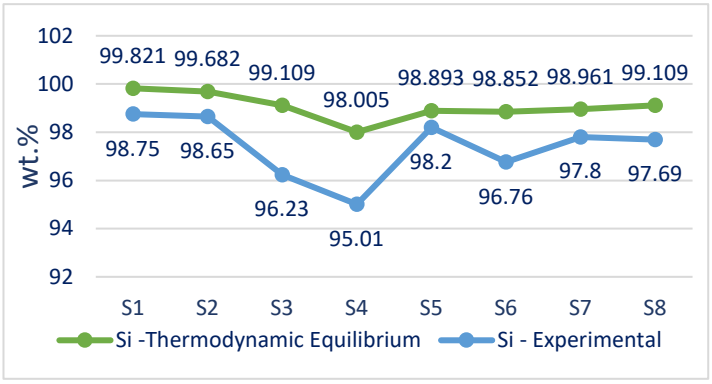

(c)

FIG 6: (a) Composition of the refined SisAl alloys refined with sculls with/without CaO, Al_2O_3 and pre-fused slag (b) Si purity with error bars indicating the variations within 3 parallels (c) comparison of the experimental and predicted values

Figure 6 (b) presents a comparative plot of the experimental and the predicted Si purity. The experimental data align well with the predicted equilibrium values; they follow the same pattern. The predicted Si content in the metal consistently match the experimental values but are generally a few percent higher than measured. Minor variations could arise from the utilization of a graphite crucible, on which a thin SiC layer is typically found after the experiments. The chemical composition analysis was conducted through multiple repetitions to ensure accuracy, and the obtained data were used to calculate error bars. In Figure 6(c), the Si content is displayed alongside these error bars. The error bars provide a visual representation of the variability in the Si content, contributing to the overall reliability and robustness of the presented results.

Figure 7 illustrates (a) macro-microscopic investigations of the refined SisAl alloys with sculls with the addition of flux and slag (b) densities of slags in the CaO-Al_2O_3-SiO_2 system.

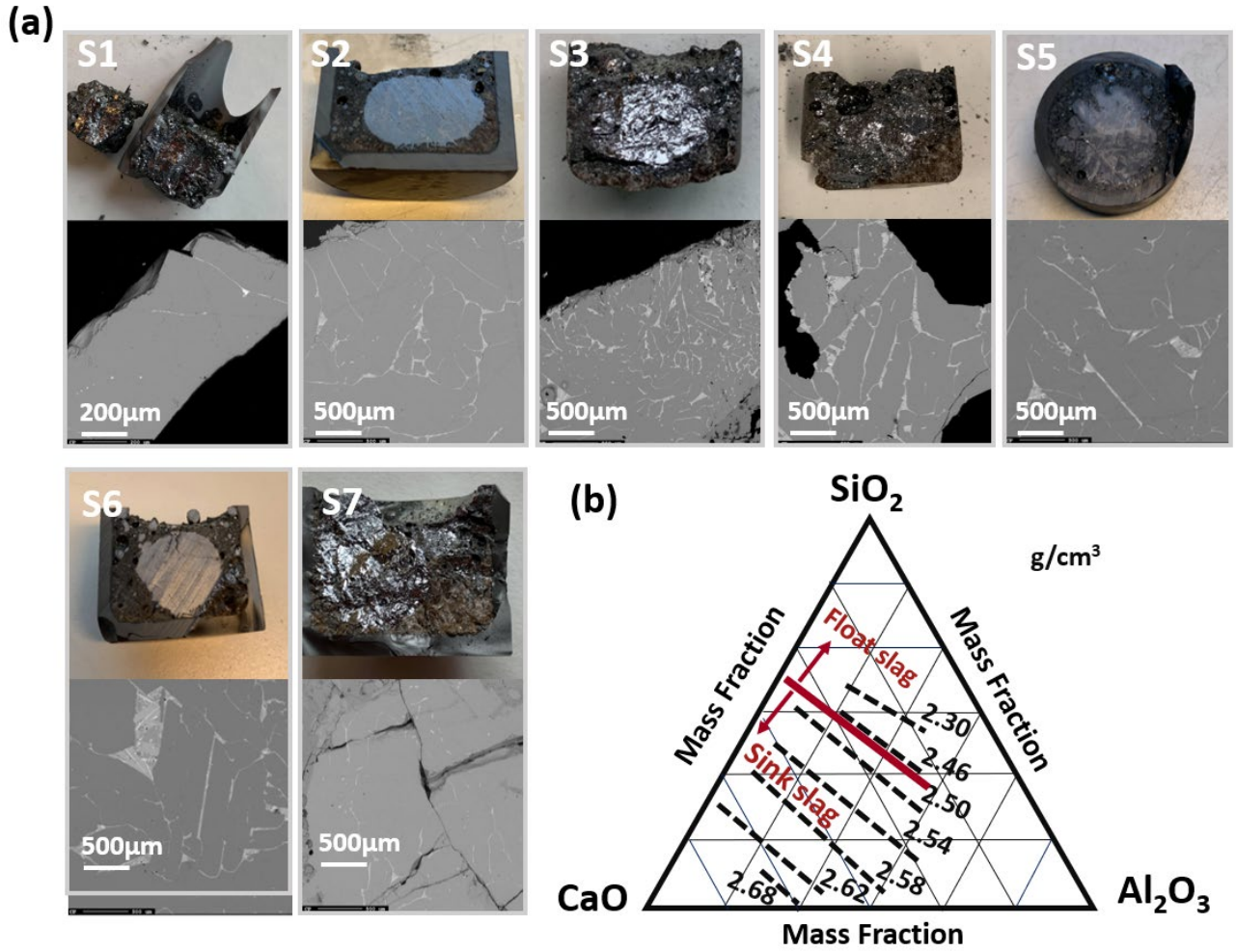

FIG 7 – (a) Macro-microscopic investigations of the refined SisAl alloys with sculls with the addition of flux and slag (b) densities of slags in the CaO-Al_2O_3-SiO_2 system at 1550°C, indicating (with red line) the density of Si compared to slags. (adapted Shei A., Tuset J K, Tveit H, 1998).

The density of pure Si in can be calculated using Equation 1. The experiments detailed in this paper were conducted at a temperature of approximately 1590°C, where the density of pure Si is found to be 2.468 g/cm³.

$$\rho(Si)_{liq} = 2533 - 0{,}45(T - T_m)\left[\frac{kg}{m^3}\right] \qquad Eq.1$$

The densities of the slags and Si are generally very similar. As seen in Figure 7 (b), higher CaO content increases slag density. Therefore, the section focused on assessing the effects of adding CaO to improve the separation between slag and metal.

In the first experiment, a mixture of 10g of SisAl alloy and 30 grams of sculls was prepared without any additional additives. As observed in the crucible picture, the separation between the metal and slag was not very successful due to the very close densities of the slag and metal. In the S2, S3, S4 and S6, CaO was added to promote better slag and metal separation. Notably, the separation of the sample from the crucible was easier, indicating that the addition of CaO had positive effect on slag and metal separation. An addition of 2g CaO and 2g Al_2O_3 was tried in sample S7 and the metal phase in S7 was clear in the picture, and it had shifted towards the left-hand side of the crucible wall in the image. This can be attributed to the interfacial tension between the slag and the metal. Thus, slag and metal separation is not solely dependent on density but is also significantly influenced by interfacial tension (Bjørnstad and Tranell, 2021).

Large-Scale Refining

Demonstration the scalability of the slag refining process of SisAl metal produced through aluminothermic reduction, represented a notable advancement from the previously successful tests conducted on a laboratory scale. The refining of SisAl metal on a large scale used 90 kg of SisAl metal along with 180 kg of sculls and 9kg of $CaCO_3$. A total of between 100 and 110 kg of metal and approximately 180 kg slag was produced. Figure 7 illustrates image and schematic representation of the furnace depicting the structure, dimensions, and positioning of components within the furnace.

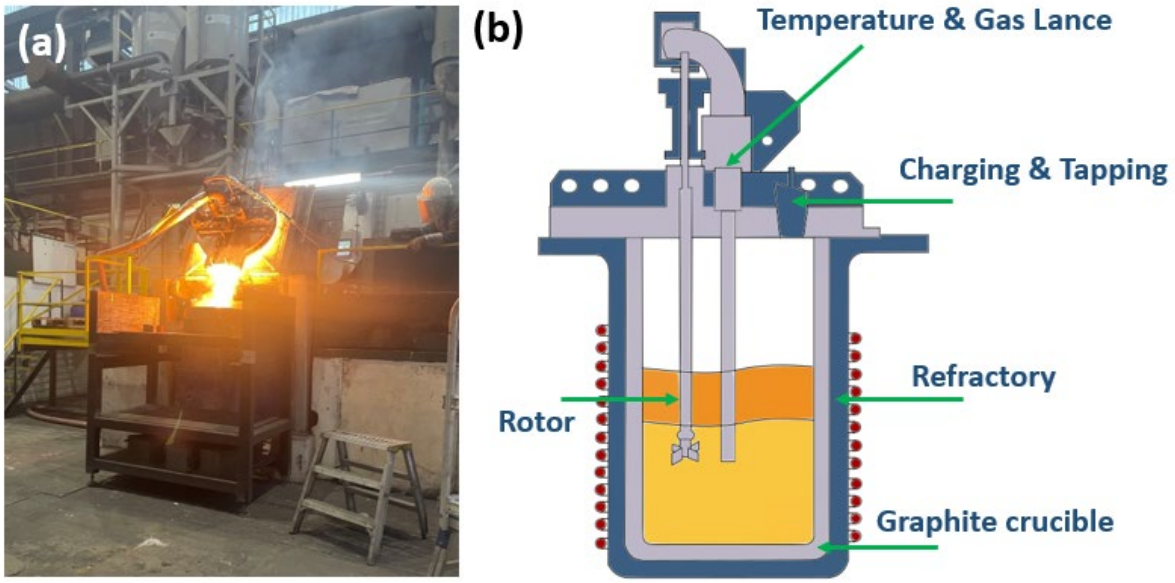

FIG 7 – Image and schematic representation of the furnace depicting the structure, dimensions, and positioning of components within the furnace.

Figure 8 illustrates composition of (a) the refined alloys and predicted values and (b) composition of slag and predicted values (d) material flow analysis for large scale slag refining.

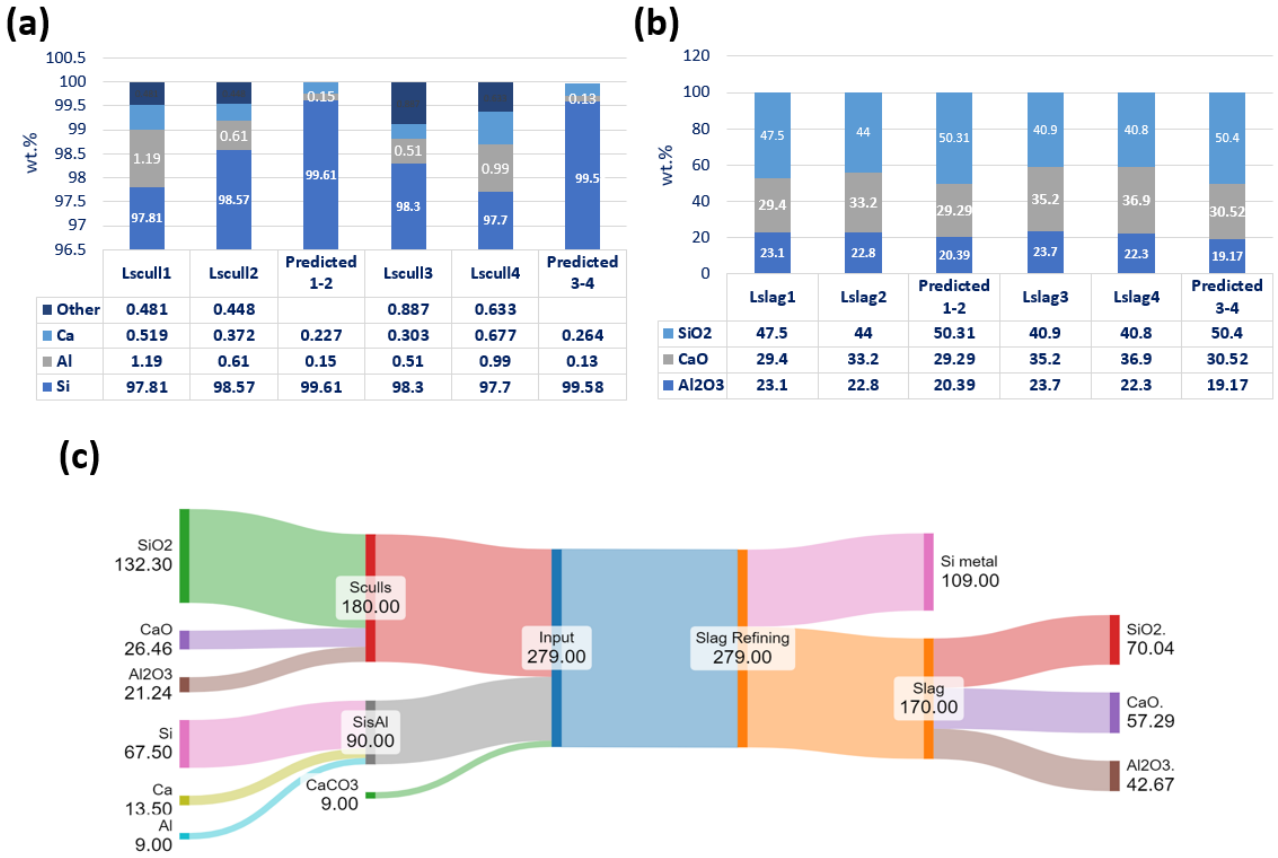

FIG 8 – Composition of (a) the refined alloys and predicted values and (b) composition of slag and predicted values (c) material flow analysis for the large-scale refining process.

Two different sculls: metal: $CaCO_3$ ratios of 2:1:0.1 and 2:1:0.2, were examined, yielding Si with a purity ranging from approximately 97.7 wt.% to 98.5 wt.%, respectively. There is no notable difference observed between the two different ratios.

The experimental data closely matches the predicted Si purity equilibrium values, however, the expected SiO_2 content in the slag was anticipated to be higher than the obtained values, indicating that a higher amount of Si than initially predicted oxidized and transferred into the slag phase. Repeated experiments under the same conditions consistently yielded similar results.

A simple mass flow analysis was conducted for the large-scale refining process, illustrated by a Sankey diagram in Figure 8. The slag refining process starts with 279 kg of materials, encompassing SisAl, sculls, and $CaCO_3$. Following the slag refining process under specified conditions, performing sculls:metal:$CaCO_3$ ratios at 2:1:0.1, the output was the production of 109 kg of Si metal and 170 kg of slag.

CONCLUSIONS

In this study, extensive laboratory-scale and large-scale refining experiments were conducted to assess the scalability and validity of the slag refining process for SisAl metal. This innovative approach is designed for the sustainable production of Si and alumina using side streams from the Si and Al industry. The experiments offered valuable insights into the effects of slag composition (anorthosite, magnetically separated anorthosite, and sculls) holding time (10, 20, 30, 40, 60 min), and additions of CaO and Al_2O_3 on the purity of refined Si metal, providing crucial information for potential industrialization. The main outcomes of this study can be summarized as follows.

1) In the laboratory-scale investigations, a range of slag compositions, including anorthosite, magnetically separated anorthosite, and sculls, were examined. Regardless of the holding time, these slag compositions consistently resulted in Si purity exceeding 96 wt.%, with the highest purity approaching 99 wt.%.

2) The addition of CaO to the refining slag facilitated better separation between metal and slag phases due to lower viscosity and higher density of the slag, though it led to a higher presence of impurities in the Si metal.

3) There was acceptable alignment between the chemical composition analysis and the thermodynamic assumptions made using FactSage 8.2.

ACKNOWLEDGEMENTS

The project (SisAl Pilot, (https://www.sisal-pilot.eu)) has received funding from the European Union's Horizon 2020 research and innovation program under Grant Agreement N° 869268.

REFERENCE

Bjørnstad E L, and Tranell G., 2021. Nucleation of SiO2-CaO-Al2O3 slag in oxidative ladle refining of metallurgical grade silicon. Metallurgical and Materials Transactions B, 52(3), 1392-1412.

Bjørnstad E L, Jung I H, Van Ende M A, & Tranell G, 2022. Oxidative refining of metallurgical grade silicon: lab-scale measurements on the overarching refining behavior of Ca and Al. Metallurgical and Materials Transactions B, 53(2), 1103-1111.

Dong Q, Lv H, 2021. Research status and prospect of high silicon aluminum alloys. Light Alloy Fabrication Technology, 49:11–16.

Engh T A, Sigworth G K, Kvithyld A, 2021. Principles of Metal Refining and Recycling Engh, T. A., Sigworth, G. K., & Kvithyld, A. (2021). Oxford University Press.

Fang M, Lu C H, Huang L Q, Lai H X, Chen J, Li J T, Ma W H, Xing P F, Luo X T, 2014. Separation of metal impurities from metallurgical grade silicon via Cao-SiO2-CaF2 slag treatment followed by leaching with hydrochloric acid. Separation Science and Technology, 49(14): 2261–2270.

Hsu C, Wu J, Lu Y, 2014. Fabrication and characteristics of black silicon for solar cell applications: An overview. Materials Science in Semiconductor Processing 25:2–17.

Hassan S, 2020. Distribution of Aluminum and Calcium between Silicon and CaO-Al2O3-SiO2 Slags at 1650°C. Master Thesis, NTNU, Trondheim.

Hosseinpour A, Tafaghodi Khajavi, L., 2018, Slag refining of silicon and silicon alloys: a review. Mineral Processing and Extractive Metallurgy Review, 39(5), 308-318.

Hoseinpur A, and Safarian J., 2021. Vacuum refining of silicon at ultra-high temperatures. Vacuum, 184, 109924.

Jakobsson L K, Tangstad M, 2014. Distribution of boron between silicon and CaO-MgO-Al 2 O 3-SiO2 slags. Metallurgical and Materials Transactions B, 45, 1644-1655.

Johnston M D, Barati M, 2010, Distribution of impurity elements in slag–silicon equilibria for oxidative refining of metallurgical silicon for solar cell applications. Solar energy materials and solar cells, 94(12), 2085-2090.

Kero I, Næss M K, Andersen V, & Tranell G M 2015. Refining kinetics of selected elements in the industrial silicon process. Metallurgical and Materials Transactions B, 46, 1186-1194.

Martorano M D A, Neto J F, Oliveira T S, Tsubaki T O, 2011. Refining of metallurgical silicon by directional solidification. Materials Science and Engineering: B, 176(3), 217-226.

PV magazine, 2022. https://www.pv-magazine.com/2022/07/29/the-pv-industry-needs-12-times-more-polysiliconproduction-capacity-by-2050/.

Ren Y, Wang H, Morita, K. 2018. Growth control and enrichment of Si crystals from Si-Sn melt by directional solidification. Vacuum, 158, 86-92.

Safarian J, Tangstad M, 2012). Kinetics and mechanism of phosphorus removal from silicon in vacuum induction refining. High Temperature Materials and Processes, 31(1).

Shei A., Tuset J K, Tveit H, 1998. Production of High Silicon Alloys, Tapir akademisk forlag.

Solar PV, IEA, Paris, 2022. https://www.iea.org/reports/solar-pv.
Sævarsdottir G, Kvande H, Magnusson T. 2021. Greenhouse gas emissions from silicon production-development of carbon footprint with changing energy systems. In Proceedings of the 16th International Ferroalloys congress (INFACON XVI).

Taeko A, Fu X, 2019. Materials: Silicon and beyond. Sensors and actuators a physical 296:340–351.

Tan Y, Guo X L, Shi S, Dong W, Jiang D C, 2013. Study on the removal process of phosphorus from silicon by electron beam melting. Vacuum, 93: 65–70.

Teixeira L A V, Morita K, 2009. Removal of boron from molten silicon using CaO–SiO2 based slags. ISIJ international, 49(6), 783-787.

Yoo B R, Jung I N, 2004 Synthesis of organosilicon compounds by new direct reactions. Advances in Organometallic Chemistry, 50, 145-179.

Zhang H, Wang Z, Ma W H, Xie K Q, Hu L, 2013. Chemical cracking effect of aqua regia on the purification of metallurgical-grade silicon. Industrial & Engineering Chemistry Research, 52(22): 7289–7296.

Zhang L, Tan Y, Li J, Liu Y, & Wang D, 2013. Study of boron removal from molten silicon by slag refining under atmosphere. Materials science in semiconductor processing, 16(6), 1645-1649.

Zheng S S, Engh T A, Tangstad M, Luo X T, 2011. Numerical simulation of phosphorus removal from silicon by induction vacuum refining. Metallurgical and Materials Transactions A, 42(8): 2214–2225.

Zhou Q, Wen J, Wu J, Ma W, Xu M, Wei K, Xu, J. 2019. Recovery and purification of metallic silicon from waste silicon slag in electromagnetic induction furnace by slag refining method. Journal of Cleaner Production, 229, 1335-1341.

Zhu M, Yue S, Wu G, Tang K, Xu Y, Safarian, J. 2021. P removal from Si by Si-Ca-Al alloying-leaching refining: Effect of Al and the CaAl2Si2 phase. Separation and Purification Technology, 271, 118675.

Zhu M, Yue S Y, Tang K, Safarian J, 2020. New insights into silicon purification by alloying–leaching refining: A comparative study of Mg–Si, Ca–Si, and Ca–Mg–Si systems. ACS Sustainable Chemistry & Engineering, 8(42), 15953-15966.

Wei D, Kong J, Zhang Z, Xing P, Zhuang Y, 2023. Study on recycling Si from silicon diamond-wire saw cutting waste by a slag refining process in industrial scale. Journal of Cleaner Production, 398, 136557.